Vol 10 No 6, June 2001
1009-1963/2001/10(06)/0516-07

Chinese Physics

© 2001 Chin. Phys. Soc.
and IOP Publishing Ltd

AN ANALYTIC MODEL FOR TRANSIENT COLLISIONAL X-RAY LASERS*

Li Ying-jun(李英骏)[a], Zhang Jie(张 杰)[a], and Teng Ai-ping(滕爱萍)[b]
[a] *Laboratory of Optical Physics, Institute of Physics, Chinese Academy of Sciences, Beijing* 100080, *China*
[b] *Department of Physics , China University of Mining & Technology, Beijing* 100083, *China*

(Received 12 February 2001)

A set of similarity equations is derived to describe the hydrodynamics of transient X-ray lasers from slab plasmas generated by combined irradiation of nanosecond and picosecond laser pulses. By separating nanosecond and picosecond laser heating processes into different periods, analytical solutions are obtained for the similarity equations. The calculated results are in agreement with numerical simulations and experimental data.

Keywords: X-ray lasers, laser plasma
PACC: 4255V, 4260

I. INTRODUCTION

Since X-ray lasing was first demonstrated in 1985,[1] much effort has been made in enhancing X-ray laser efficiency and developing "table-top" X-ray lasers for applications. Recent studies show that the "traditional" collisional X-ray lasers in the quasi-steady state (QSS) regime can be pumped by optical lasers with energies of less than 100 J.[2] Wavelengths of saturated X-ray lasers are approaching the "water window".[3] The improvement of efficiency and the saturated output were achieved by relaxing refraction through the use of the prepulse technique.[4,5]

On the other hand, a novel transient collisional excitation (TCE) scheme was demonstrated recently for the Ne-like Ti ions on the 3p–3s (J=0→1) transition at 32.6nm, where a high gain of 19cm^{-1} was measured with only a few Joules drive energy.[6] Later experiments showed a gain of 35cm^{-1} and a gL product of 12.5 on the 4d–4p (J=0→1) transition at 14.7nm for the Ni-like Pd ions using a pump energy of only 5 J.[7] Saturation of the transient Ne-like Ti and Ne-like Ge X-ray lasers was achieved using a low pump energy.[8,9]

Until now, the design and analysis of TCE X-ray lasers have relied heavily on numerical simulations of hydrodynamics and atomic kinetics.[10] In this paper, we show an analytical model to describe the hydrodynamics of transient collisional excitation X-ray lasers. The purpose of our work is to understand the physical process of the transient collisional X-ray lasers and to help the quick design of X-ray laser experiments. We derive similarity equations and ionization relations in section II and show the analytic solutions in section III. The results are analysed and discussed in section IV. The validity of the model is discussed in section V. An experiment of transient collisional Ne-like Cr X-ray laser is designed using this model in section VI. And finally, conclusions are given in section VI.

II. BASIC PRINCIPLE OF TRANSIENT COLLISIONAL EXCITATION

A. Basic process of transient collisional excitation and similarity equations

In the "traditional"collisional scheme, X-ray lasers mainly operate in the QSS scheme. For example, in the case of Ne-like ions with a closed shell with a ground-state configuration of $1s^22s^22p^6$, the 3p upper laser levels are populated principally through direct monopole collisional excitation from the ground state, while the 3s lower levels are radiatively connected with the ground state. Inversion then occurs between 3p and 3s levels as a result of the different rates of radiative decay. However, the electron temperature required for an optimum collision rate to populate the 3p upper laser levels is too high to allow a significant steady-state population of Ne-like ions to exist,[11] because the plasma would be overionized at too high a temperature. The QSS scheme is thus inefficient, as energy is wasted through the stripping of ions beyond the desired state of charge. The TCE scheme differs

*Project supported by the National Natural Science Foundation of China (Grant Nos. 19974074 and 19825110) and by the National High Technology High Power Lasers Program of China, and by the National Key Basic Research Special Foundation (NKBRSF), China (Grant No. G1999075200).

from the QSS in a number of respects, but mainly because the pump pulse in the TCE is shorter than the thermalization time between ions and electrons. The fast pump causes transient population inversion directly from the ground state while keeping a low ion temperature.[7]

Experimentally, the TCE scheme involves a combinative irradiation of nanosecond and picosecond optical laser pulses. The nanosecond pulse heats a target to produce a long scale length plasma with Ne-like (or Ni-like) ionization stage. Depending on the required initial temperature, degree of ionization, electron density and density gradients, a delay is essential before the arrival of the picosecond pulse. The picosecond pump pulse then rapidly heats up the plasma with a sudden increase in electron temperature to reach $T_{\rm e} \geq \Delta E_{\rm u}$, where $\Delta E_{\rm u}$ is the upper laser level energy.

Usually, a slab plasma can be divided into cold region, radiation thermal conductive region, electron thermal conductive region, corona region (laser absorption region) and flying-off region. The X-ray laser gain can only be generated in the corona region of $n_{\rm e} < n_{\rm c}$ ($n_{\rm e}$ is the electron density, $n_{\rm c}$ is the critical density ($\approx 1.1 \times 10^{21}/\lambda^2 {\rm cm}^{-3}$)). The following analysis will be carried out in this region. In this region, electrons and ions have different temperatures, and their velocity distribution reaches different Maxwellian, respectively. Because the mass of the ions is much heavier than that of electrons, we assume that the ions serve as a background of electrons. We assume that the plasma is an ideal gas. Thus a single fluid, ideal gas hydrodynamic equation can be adopted:

$$\frac{\partial \rho}{\partial t} + \frac{\partial \rho \nu}{\partial x} = 0, \tag{1}$$

$$\rho\left(\frac{\partial \nu}{\partial t} + \nu \frac{\partial \nu}{\partial x}\right) = -\frac{\partial p}{\partial x}, \tag{2}$$

$$\frac{\partial}{\partial t}\left[\rho\left(\varepsilon + \frac{\nu^2}{2}\right)\right] = -\frac{\partial}{\partial x}\left[\rho\nu\left(\varepsilon + \frac{\nu^2}{2}\right) + p\nu\right] + \rho H, \tag{3}$$

where x is the spatial coordinate perpendicular to the slab surface, t is the time, ρ, ν, p and T are the mass density, velocity, pressure and temperature, respectively, ε is the internal energy per unit mass and H is the net heating rate per unit mass. The equation of state and the laser heat deposition are discussed as follows.

In order to obtain the similarity equations we assume that the expansion of the plasma is homogeneous and satisfies the rarefactional wave solution varying with time:

$$\nu = C_{\rm s} + x/t, \tag{4}$$

where $C_{\rm s}$ is the transient isothermal sound speed [$C_{\rm s} = \sqrt{TZ/M_i} = T^{1/2}Z^{1/2}/M_i^{1/2}$]. The momentum equation [Eq.(2)] can be separated in space and time under these assumptions. The solution of the spatial part (at constant time) gives an exponential density profile, which is normalized by the continuity equation

$$\rho = (m/L)\exp(-x/L), \tag{5}$$

where m is the mass ablated from the slab target by the nanosecond (ns) laser pulse, L is the scale length of the plasma. With the equation of the mass ablation rate derived by De Groot *et al*,.[12] which is valid for the ablation process of the thick slab target irradiated by the ns laser pulse, the relation can be derived among the ablation mass, the intensity of the drive laser and the target element under the assumption of an homogeneous ablation

$$m = 2.55 \times 10^{-13} I^{2/3} t^{2/3} [A/(Z+1)]^{7/6}/(Z \ln \Lambda)^{1/3}, \tag{6}$$

where the unit of m is g/cm^2, the unit of t is ns, the unit of I is W/cm^2, A is the atomic number of the element, Z is the average charge of the ion and $\ln\Lambda$ is the natural Coulomb logarithm. With the assumption of the homogeneous expansion, the momentum and energy equations can be simplified as

$$LC_{\rm s}\left(\frac{t}{2}\frac{{\rm d}\ln T}{{\rm d}t} + 1\right) = \frac{pt}{\rho}, \tag{7}$$

$$C_\nu \frac{{\rm d}T}{{\rm d}t} = H - \frac{p}{\rho t}, \tag{8}$$

where $C_\nu (\equiv {\rm d}\varepsilon/{\rm d}T)$ is the specific heat per unit mass.

B. The laser heating term, ionization and equation of state

In our model, the laser energy is mainly deposited in the corona region (near $n_{\rm c}$) through the inverse bremsstrahlung in the incident direction of the drive laser perpendicular to the surface of the slab. We distribute the energy equally per unit mass through the plasma and ignore the laser reflection at the critical surface since we are only interested in the corona region, where the gain is generated. We assume that the main absorption process during the interaction of the laser pulse and the corona plasma is the inverse bremsstrahlung.[13] The heating rate is determined from the absorbed fraction of laser flux[14]

$$H = (1/m)\ [I(s) - I] = (I/m)\ [1 - \exp(\tau_{\rm iB})], \tag{9}$$

where I is the total laser flux through the plasma, s is the coordinate of laser incidence direction and $\tau_{\rm iB}$ is the inverse bremsstrahlung optical depth through the plasma:

$$\tau_{\rm iB} = \int \kappa_{\rm iB} {\rm d}x. \tag{10}$$

The opacity $\kappa_{\rm iB}$ is determined by the following formula:[15]

$$\kappa_{\rm iB} = \left(\frac{2}{\pi}\right)^{1/2} \frac{4}{3} \left(\frac{Z n_{\rm e}^2 e^6 (\log \Lambda) \lambda^2}{c^3 (m_{\rm e} T)^{3/2} (1 - n_{\rm e}^2/n_{\rm c}^2)^{1/2}}\right), \tag{11}$$

where λ is the laser wavelength, $n_{\rm e}$ is the electron density, $n_{\rm c}$ is the critical density, T is the electron temperature in energy unit, Z is the average ion charge, $m_{\rm e}$ is the electron mass and c is the light velocity.

For the corona region of $n_{\rm e} \leq n_{\rm c}$, the electron temperature is higher than a few tens of eV. The corona model may be used in the following relation:[16]

$$Z \approx \frac{2}{3} [A T_{\rm e}({\rm eV})]^{1/3}, \tag{12}$$

where A is the atomic number of the element.

The equation of state and heat capacity (EOS quantities) will be discussed in section III.

Ⅲ. ANALYTIC SOLUTIONS OF THE SIMILARITY EQUATIONS

Useful scaling laws for the plasma variables are derived from analytic solutions for flat-top laser pulses in this section. To obtain analytic solutions, we assume the Coulomb logarithm in the laser heating term to have a constant value. We choose a constant $\log\Lambda$ between 4 and 5 in our calculation, from the comparison with the numerical calculation of JB19[17,18] and Medusa,[19] for the temperature and density of interest. The input parameters of the solutions are I, λ, m and A for the long pulse and I, λ, m, A and Z for the short pulse, while the output variables are T and L. The density at a position x is determined by m and A for the long pulse and by m, A and Z for the short pulse. We employed in the following calculation convenient units in table 1, similar to Ref.[14].

Table 1. Normalized values for scaled variables.

Physical variable	Symbol	Normalized value
Time	t	1 ns
Laser intensity	I	10^{14} Wcm^{-2}
Laser wavelength	λ	1.053μm
Ablation mass	m	10^{-4}gcm^{-2}
Ion charge	Z	25
Atomic mass	A	80
Coulomb logarithm	Λ	5

A. Analytic solutions for the long pulse

The main purpose for the long pulse is to produce a long scale length plasma with optimized initial temperature, electron density, density gradients, and especially Ne-like ionization stage. The heating and ionization processes take place for the whole pulse duration. In the isothermal expansion stage of the corona region of $n_{\rm e} < n_{\rm c}$, the heating rate changes with $\tau_{\rm iB}$, i.e. $H \approx I\tau_{\rm iB}/m$, for the long pulse because the plasma is optically thin for the incident laser. From Eq.(12), the EOS is written as

$$p = \frac{2}{3({\rm eV})^{1/3}} \frac{A^{1/3} T^{4/3} \rho}{M_{\rm i}},$$
$$C_\nu = \frac{A^{1/3} (T/{\rm eV})^{1/3}}{M_{\rm i}}. \tag{13}$$

An expression for the optical depth is obtained by integrating Eq.(10) over the density profile since the heating and ionization processes take place in the region where the electron density is close to the critical density,[16]

$$\tau_{\rm iB} = 2.75\sqrt{\pi} \times 10^{-4} \underline{m}^2 \underline{A}^2 \underline{Z}^3 \underline{\Lambda\lambda}^2 T^{3/2} L, \tag{14}$$

where Λ is taken as a constant value in the corona. We solve Eqs.(7) and (8) with (13) and (14). After the influence of the initial condition disappears, the analytic solutions are

$$T = 1.44{\rm keV} \underline{I}^{5/9} \underline{A}^{2/9} \underline{\Lambda}^{2/9} \underline{\lambda}^{2/3} \underline{t}^{2/3}, \tag{15a}$$

$$L = 1.90 \times 10^{-2} {\rm cm} \underline{I}^{10/27} \underline{A}^{-2/27} \underline{\lambda}^{4/9} \underline{\Lambda}^{4/27} \underline{t}^{31/27}, \tag{15b}$$

$$n_0 = 4.93 \times 10^{20} {\rm cm}^{-3} \underline{I}^{11/54} \underline{A}^{4/27} \underline{\lambda}^{-5/9} \underline{\Lambda}^{-2/54} \underline{t}^{-14/27}, \tag{15c}$$

here n_0 is the maximum value of $n_{\rm e}$. Using Eq. (5), we can determine the electron density at position x and time t with (15c).

This period is most important for optimizing the plasma conditions. From Eq.(12), the state of charge Z is proportional to one-third the power of the temperature.

B. Analytic solutions for the short pulse

The transient population inversion is created by rapid heating. The heating time should be so short that the timescale is shorter than that of the relaxation processes of the excited states and any significant further ionization cannot occur.[9] The preplasma is not transparent for the short pulse since the transparent temperature is proportional to three-fourths the power of the intensity at the early time.[19]

It can be assumed that m is constant after the time $t_{1\mathrm{L}}$ and the heating rate is taken as constant at early times because the plasma is optically thick for the incident short laser pulse. Secondly, there is almost not enough time to change the state of ion charge. This means that Z can be taken as a constant. The formulae we use for the EOS here are

$$p = ZT\rho/M_{\mathrm{i}} \text{ and } C_\nu = \frac{3}{2}Z/M_{\mathrm{i}}, \tag{16}$$

where M_{i} is the ion mass.

1. During the time interval $t_{1\mathrm{L}} \le t \le t_{2\mathrm{L}}$

After the nanosecond pulse laser is turned off and the picosecond laser pulse starts at time $t_{1\mathrm{L}}$, the solutions can be obtained by considering the initial conditions before $t_{1\mathrm{L}}$:

$$T = 20.04\mathrm{keV}\underline{I_2}\underline{m}^{-1}\underline{AZ}^{-1}\underline{t}\left(1 - t_{1\mathrm{L}}^{5/3}t^{-5/3} + \frac{T_{1\mathrm{L}}t_{1L}^{2/3}}{20.04I_2m^{-1}AZ^{-1}}t^{-5/3}\right), \tag{17a}$$

where $T_{1\mathrm{L}}$ is the electron temperature at $t_{1\mathrm{L}}$.

$$L = 5.17\times10^{-2}\mathrm{cm}\underline{I_2}^{1/2}\underline{m}^{-1/2}\underline{t}^{3/2}\cdot\left(1 - t_{1\mathrm{L}}^{5/3}t^{-5/3} + \frac{L_{1\mathrm{L}}^2t_{1L}^{2/3}}{L_2^2}t^{-5/3}\right)^{1/2}, \tag{17b}$$

where $L_{1\mathrm{L}}$ is the scale length at $t_{1\mathrm{L}}$, $L_2 = 5.17\times10^{-2}\mathrm{cm}\underline{I_2}^{1/2}\underline{m}^{-1/2}$.

$$n_0 = 3.64\times10^{20}\mathrm{cm}^{-3}\underline{I_2}^{-1/2}\underline{m}^{3/2}\underline{A}^{-1}\underline{Zt}^{-3/2}\cdot\left(1 - t_{1\mathrm{L}}^{-5/3}t^{-5/3} + \frac{n_2^2}{n_{1\mathrm{L}}^2t_{1\mathrm{L}}^{2/3}}t^{-5/3}\right)^{-1/2}, \tag{17c}$$

where $n_{1\mathrm{L}}$ is the electron density at $t_{1\mathrm{L}}$, $n_2 = 3.64\times10^{20}\mathrm{cm}^{-3}\underline{I_2}^{-1/2}\underline{m}^{3/2}\underline{A}^{-1}\underline{Z}$. This period is more important to enhance the gain.

2. During the time $t_{2\mathrm{L}} \le t$

After the time $t_{2\mathrm{L}}$, the short laser pulse is turned off and the plasma continues to expand adiabatically. The analytical solutions are obtained for this period by using the conditions before $t_{2\mathrm{L}}$:

$$T = 20.04\mathrm{keV}I_2m^{-1}\underline{AZ}^{-1}\underline{t}_{2L}^{5/3}\underline{t}^{-2/3}\cdot\left(1 - t_{1\mathrm{L}}^{5/3}t_{2\mathrm{L}}^{-5/3} + \frac{T_{1\mathrm{L}}t_{1L}^{2/3}t_{2L}^{-5/3}}{20.04c\underline{I_2}\underline{m}^{-1}\underline{AZ}^{-1}}\right), \tag{18a}$$

$$L = L_{1\mathrm{L}}t_{2\mathrm{L}}^{5/6}t^{2/3}\left(1 - t_{1\mathrm{L}}^{5/3}t_{2\mathrm{L}}^{-5/3} + \frac{L_{1\mathrm{L}}^2t_{1L}^{2/3}}{L_2^2}t_{2\mathrm{L}}^{-5/3}\right)^{1/2}, \tag{18b}$$

$$n_0 = n_{1\mathrm{L}}t_{2\mathrm{L}}^{-5/6}t^{-2/3}\left(1 - t_{1\mathrm{L}}^{-5/3}t_{2\mathrm{L}}^{-5/3} + \frac{n_2^2}{n_{1\mathrm{L}}^2t_{1\mathrm{L}}^{2/3}}t_{2\mathrm{L}}^{-5/3}\right)^{-1/2}. \tag{18c}$$

The electron temperature is dependent on two-thirds the power of time after the laser pulse is turned off. In Fig.1, one special period for the long pulse and two periods for the short pulse are shown in order to clearly indicate physical process in the calculation.

IV. RESULTS AND DISCUSSION

In order to show the reliability of the model, we calculate the hydrodynamics of the transient collisional Ne-like Ti X-ray laser using the same experimental conditions:[8] $I_1 = 1.7\times10^{12}\mathrm{W/cm}^2$, $\lambda = 1.053\mu$m, $t_{1\mathrm{L}}$=1ns, $I_2 = 2.2\times10^{14}\mathrm{W/cm}^2$, $t_{2\mathrm{L}}$=7ps and slab Ti target.

The results show that it is clear from Eq.(12) that a constant temperature is beneficial to produce abundant ions because the state of charge, Z, is proportional to one-third the power of the temperature. The electron temperature is almost constant at the late time of the long pulse and the constant temperature is about 127eV during the isothermal period (the solid line in Fig.1(a)). The average ionization of T_{i} plasma is Z=12.2. For the long pulse, the scale length here is about 50μm, shown by the solid line in Fig.1(b) and the maximum electron density is about $1.6\times10^{21}\mathrm{cm}^{-3}$. The electron density changes with time for different x as shown in Fig.1(d). The electron density is about $7.3\times10^{20}\mathrm{cm}^{-3}$ at x=20μm and t=1ns. It is efficient to use $1.7\times10^{12}\mathrm{W/cm}^2$ intensity and 1ns pulse duration for the production of Ne-like Ti ions for the long laser pulse.

For the short pulse, the $2.2\times10^{14}\mathrm{W/cm}^2$ intensity makes the electron temperature rise quickly from 127eV to 1.54keV during the 7ps pulse duration, shown by the dashed line in Fig.1 (a). This is about three times ΔE_{u}=459.7eV. Dunn *et al.*[7] showed that the electron temperature has to be at least equal to or higher than ΔE_{u}, i.e. $T_{\mathrm{e}} \ge \Delta E_{\mathrm{u}}$, where ΔE_{u} is the upper laser level excitation energy. The ion temperature could almost be regarded to be kept at a low temperature because the 7ps pulse is too short for any significant further collisional ionization to occur. This is beneficial for high gain operation because the gain coefficient is proportional to the electron temperature and inversely proportional to the square root of the ion temperature.

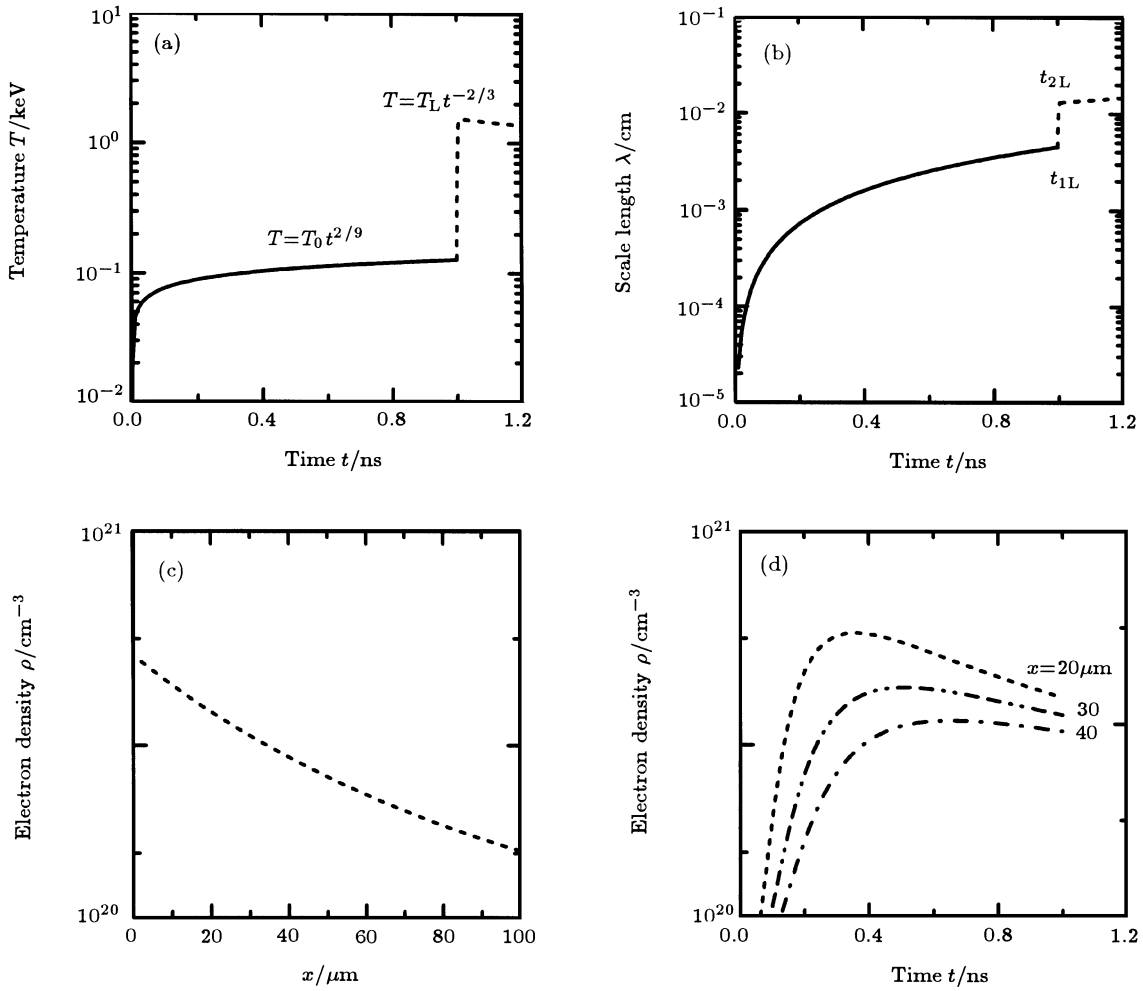


Fig.1. Temperature history (a), scale length history (b), density history for different x (d) and density curves with x (c) from the similarity equations for different long pulse duration of a flat-top pulse. The solid line is for the long pulse. The dashed line is the solution for the short pulse. The conditions of the lasers are $I_1 = 1.7 \times 10^{12}$W/cm^2, λ=1.053μm, t_{1L}=1 ns, $I_2 = 2.2 \times 10^{14}$W/cm^2, t_{2L}=7ps after t_{1L}.

The longer scale length produces a more relaxed density gradient. This is advantageous for the X-ray laser propagation. The scale length here is about 100μm at the peak time of the pulse, shown by the dashed line in Fig.1 (b). The electron density versus x is shown in Fig.1(c) and the initial electron density here is about 7.1×10^{20}cm^{-3} at the peak time of the pulse.

V. VALIDITY OF THE SIMILARITY MODEL

In this section, we discuss the validity of the similarity model by comparison with the numerical simulation.

A. Isothermality of the corona

The similarity model of slab plasmas is based on the assumption of isothermal expansion in the corona. It is well known that the laser energy is mainly deposited in the corona region of $n_e < n_c$. The simulation using JB19 code[18] and Medusa[19] prove the validity of this assumption. The assumption is more suitable at the later time for the long pulse. However, the scaling laws agree with Rosen's scaling laws for femtosecond laser–plasma interaction.[20] Thus, the model can also be used to solve the ultra-short pulse laser–plasma interactions.

In order to verify the condition of validity of the model, we compare the analytic calculations of the model with the simulation results of JB19 and Medusa for Ne-like Ge X-ray laser on single pulse, shown in Fig.2. The input parameters of simulations are I=10^{13}W/cm^2, λ=1.053μm, t_L=1.1ns for a germanium target. We can see from Fig.2 that the analytic solutions agree well with the simulations. The temperature at the later time keeps almost constant due to a balance between laser heating and expansion

cooling. The temperature is about 808 eV in the analytic solutions and 810 eV in JB19. The density at the later time is about $2.2 \times 10^{20}\mathrm{cm}^{-3}$ in the analytic solutions and $1.3 \times 10^{20}\mathrm{cm}^{-3}$ in JB19 at x=150μm. Medusa simulations also produce similar results.

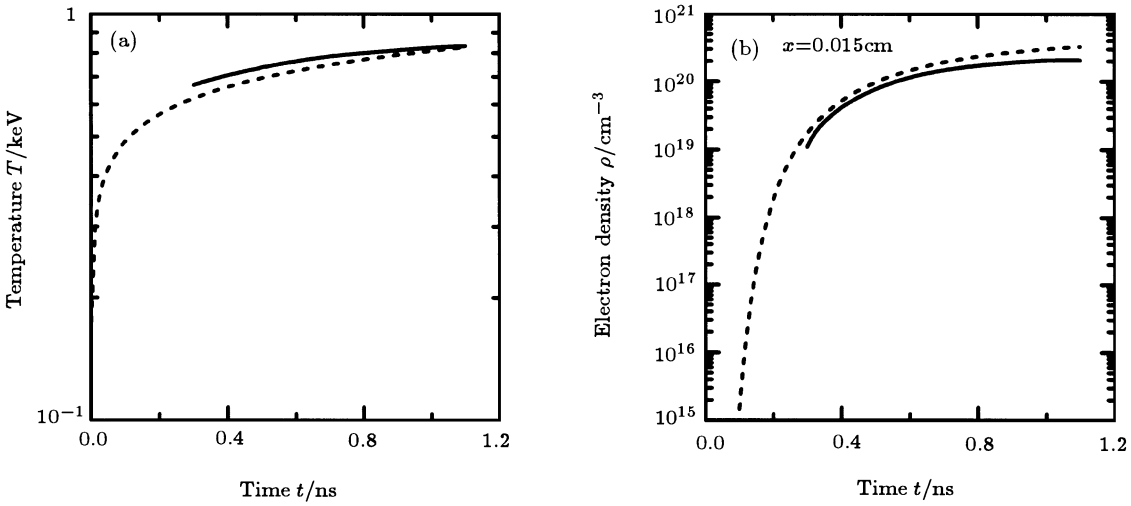


Fig.2. Temperature history (a) and density history at x=150μm (b). The solid line is the result from JB19, while the dashed lines are the analytic results from the similarity equations for a flat-top laser pulse, where $I = 10^{13}\mathrm{W/cm}^2$, λ=1.053μm, t_L=1.1 ns for slab germanium target.

B. Validity of the ablation mass equations

The mass ablation rate equation is derived by Groot *et al.*[12] with the assumption of an homogeneous ablation

$$\frac{\mathrm{d}m}{\mathrm{d}t} = 1.7 \times 10^{-4} \frac{I^{2/3}}{(Zt \log \Lambda)^{1/3}} \cdot \left(\frac{A}{Z+1}\right)^{7/6} \left[\frac{g}{\mathrm{cm}^2 \cdot \mathrm{s}}\right]. \qquad (19)$$

The ablation process of the thick slab target irradiated by the laser pulse is homogeneous since the laser pulse is flat-top. Thus, equation (6) of the ablation mass can be derived.

C. Validity of the ionization equation

In order to see if the corona model applies to the plasma here, we should scrutinize the conditions of the validity of the corona model. (a) The velocity distribution of the electrons must be Maxwellian. (b) The population density of ions of charge (Z+1) must not change significantly during the period when the quasi-steady state population distribution is established among the ions of charge Z. (c) The plasma must be optically thin. Considering the characteristic of the isothermal expansion region, the conditions can be well satisfied. However, the model is more valid for heavy elements than for light elements.[16]

D. Criteria for the duration of the short pulse

We now study the limit of pulse duration, below which the effects of the heating on ionization can be ignored. For this purpose, we estimate the thermodynamic equilibrium time between electrons and ions by the assumptions that the velocity distributions of the electrons and ions are Maxwellian and the electrons are "hot" and the ions are "cold":

$$t_\mathrm{ei} = \left(\frac{4\pi\varepsilon_0}{e^2}\right)^2 \frac{3 m_\mathrm{i} m_\mathrm{e}^{-1/2} (kT_\mathrm{e})^{3/2}}{8\sqrt{2\pi} Z^2 n_\mathrm{i} (\log \Lambda)}. \qquad (20)$$

The higher the electron temperature, the longer the equilibrium time is from the Eq.(20). We can neglect the energy exchange between electrons and ions when the ratio of the short pulse duration to the equilibrium time is smaller that 10^{-3}. For example, the ratio for the equilibrium time t_ei=11.4ns to the short pulse duration t_2L=7ps, under the conditions we consider here is 6.14×10^{-4}.

VI. APPLICATIONS AND CONCLUSION

We now study the experimental design of the Ne-like Cr X-ray laser using this model. We employ the chromium slab target because the X-ray laser output from Ne-like Cr ions has single line emission spectrum. This has more advantage over the Ne-like Ti laser, be-

cause a single line X-ray laser is more useful for the application in the plasma diagnostics.

Design calculations give electron temperature, density, ionization and electron density profile in the transient gain region. We obtain the required laser intensity and pulses duration for the long pulse for optimized electron temperature, degree of ionization and electron density and for the short pulse for optimized electron temperature and density gradients from the calculation. The results are listed in table 2. The electron density profile for the isothermal region is

Table 2. Input parameters and results.

Physical parameters	Long pulse	Short pulse
Laser wavelength	1.053μm	1.053μm
Laser intensity	3.2×10^{12}W/cm^2	2.2×10^{14}W/cm^2
Pulse duration	1 ns	10 ps
Maximum electron temperature	184 eV	1.58 keV
Degree of ionization	14.2	14.2

$$n_{\rm e} = 9.5\times10^{20}\exp(-x/106). \qquad (21)$$

For the application, the density profile of electrons can be approximated as

$$n_{\rm e} = 9.5\times10^{20}\big(1-x/106\big), \qquad (22)$$

here the unit of $n_0 = 9.5\times10^{20}$ is cm^{-3} and unit of L=106 is μm. The range of x is from 5 to 110μm outside $n_{\rm c}$. The ratio of the short pulse duration to the equilibrium time is 1.0×10^{-3}. The electron temperature is about 2.7 times $\Delta E_{\rm u}$=586eV.

In conclusion, we have developed a similarity model for transient X-ray lasers. Analytical solutions are obtained by separating the heating processes into different periods. The calculations are in good agreement with numerical simulation and experimental results. The model is useful for approximate, quick parameter studies for experimental design and analysis of experiments. Especially, it provides a useful tool to understand the physical process of the transient X-ray laser hydrodynamics.

ACKNOWLEDGMENTS

Y J Li would like to acknowledge the useful discussions with Professor J Nilsen.

References

[1] Matthews D L, Hagelstein P L, Rosen M D, Eckalrt M J, Ceglio N M, Hazi A U, Medecki H, MacGowan B J, Trebes J E, Kauffman B L, Pleasance L D, Rambach G, Scofield J H, Stone G and Weaver T A 1985 *Phys. Rev. Lett.* **54** 110

[2] Prag A, Glinz A, Balmer J E, Li Y and Fill E E 1996 *Appl. Phys. B: Laser Opt.* **63** 113

[3] Zhang J, Machee A G, Nilsen J, Lin J, Barbee Jr T W, Danson C, Key M H, Lewis C L S, Neely D, O'Rourke R M N, Pert G J, Smith R, Tallents G J, Wark J S and Wolfrum E 1997 *Phys. Rev. Lett.* **78** 3856

[4] Nilsen J, MacGowan B J, DaSilva L B and Moreno J C 1993 *Phys. Rev.* A **48** 4682

[5] Zhang J, Machee A G, Lin J, Wolfrum E, Smith R, Danson C, Key M H, Lewis C L S, Neely D, Nilsen J, Pert G J, Tallents G J and Wark J S 1997 *Science* **276** 1097

[6] Nickles P V, Shlyaptsev V N, Kalachnikov M, Schnürer M, Will I and Sandner W 1997 *Phys. Rev. Lett.* **78** 2748

[7] Dunn J, Osterheld A L, Shepherd R, White W E, Shlyaptsev V N and Stewart R E 1998 *Phys. Rev. Lett.* **80** 2825

[8] Kalachnikov M P, Nickles P V, Schnürer M, Sandner W, Shlyaptsev V N, Danson C, Neely D, Wolfrure E, Zhang J, Behjat A, Demir A, Tallents G J, Warwick P J and Lewis C L S 1998 *Phys. Rev.* A **57** 4778

[9] Warwick P J, Lewis C L S, Kalachnikov M P, Nickles P V, Schnürer M, Behjat A, Demir A, Tallents G J, Neely D, Wolfrum E, Zhang J and Pert G J 1998 *J. Opt. Soc. Am.* B **15** 1808

[10] Nilsen J, Li Y and Dunn J 2000 *J. Opt. Soc. Am.* B **17** 1084

[11] Afanasiev Yu V and Shlyaptsev V N 1989 *Sov. J. Quantum Electron.* **19** 1606

[12] De Groot J S, Estabrook K G and Kruer W L *et al* 1992 *Phys. Fluids* B **4** 701

[13] Dawson J M 1964 *Phys. Fluids* **7** 981

[14] London R A and Rose M D 1986 *Phys. Fluids* **29** 3813

[15] Johnston T W and Dawson J M 1973 *Phys. Fluids* **16** 722

[16] Colombant D and Tonon G T 1973 *J. Appl. Phys.* **44** 3524

[17] Li Y J and Zhang J 2001 *Phys. Rev.* E **63** 036410

[18] Li Y J, Zhang G P, Zhang J and Peng H S 1999 *Chin. J. Comput. Phys.* **16** 37 (in Chinese)

[19] Zhang J, Key M H, Rose S J and Tallents G J 1994 *Phys. Rev.* A **49** 4024

[20] Rosen M D 1990 *Proc. SPIE* **1229** 160